Natural Hazards and Earth System Sciences

Open Access

EGU

Discussions

1

2

Modeling ground deformation associated with the destructive earthquakes occurring on Mt. Etna's southeastern flank in 1984

5

6

Flavio Cannavò[1], Salvatore Gambino[1], Biagio Puglisi[2], Rosanna Velardita[2]

[1]*Istituto Nazionale di Geofisica e Vulcanologia, - Osservatorio Etneo, Piazza Roma 2, Catania, Italy*

[2]*Istituto Nazionale di Geofisica e Vulcanologia, - Osservatorio Etneo, Via Monti Rossi, 95123 Nicolosi (CT), Italy*

10

11

Submitted to Natural Hazards and Earth System Sciences

13

14

15

Correspondence to:

17

Dr. Salvatore Gambino
Istituto Nazionale di Geofisica e Vulcanologia
Sezione di Catania Osservatorio Etneo
P.zza Roma 2, 95123 Catania, Italy
tel. number 39-95-7165877
fax number: 39-957165826
e-mail: Salvatore.gambino@ingv.it

25

26

27

28

Natural Hazards
and Earth System
Sciences

Discussions

Open Access

EGU

29   **Abstract**

30   The Timpe Fault System is the source of very shallow but destructive earthquakes that affect

31   several towns and villages on the eastern flank of Mt. Etna (Italy). In 1984, several seismic events,

32   and specifically on October 25, caused one fatality, 12 injuries and produced serious damage in the

33   Zafferana and Acireale territories. This seismicity was mainly related to the activity of the Fiandaca

34   Fault, one of the structures belonging to the Timpe Fault System.

35   We inverted ground deformation data collected by a geodimeter trilateration network set up in 1977

36   at a low altitude along the eastern side of the volcano in order to define the Timpe Fault System

37   faulting mechanisms linked to the seismicity in 1984.

38   We found that in the May 1980-October 1984 period, the Fiandaca Fault was affected by a strike

39   slip and normal dip slip of about 27 and 23cm. This result is in fairly good accord with field

40   observations of the co-seismic ground ruptures along the fault but it's notably large compared to

41   displacements estimated by seismicity, then suggesting that most of the slip over the fault plane was

42   aseismic.

43   The results once again confirm how seismicity and in particular ground ruptures represent a very

44   high hazard to the several towns and villages situated along the Fiandaca Fault.

45   ***Keywords:*** *Geodetic observations, flank dynamics, fault displacements, shallow earthquakes*

46

47   **1.0 Introduction**

48   The determination of finite fault geometry and slip for severe earthquakes is important for the

49   mitigation of seismic hazard and in particular for very shallow earthquakes that entail surface

50   fracturing.

51   On the eastern flank of Etna volcano, movements along very shallow normal faults generate

52   recurrent seismicity sometimes leading to destructive events, since densely urbanized areas are

53 located on these structures (e.g. Azzaro et al., 2012; Barreca et al., 2013c). The Timpe Fault System

54 (TFS) is the main source generating the strongest earthquakes known over the last 200 years

55 (Azzaro et al., 2012).

56 The TFS dissects the southern-eastern flank of Mt. Etna (Fig. 1) and is formed by several fault

57 segments that include the Fiandaca (FF), S. Tecla (STF), S. Venerina (SVF), Moscarello (MF) and

58 San Leonardello (SLF) faults (fig. 2B), generally characterized by normal and right-lateral

59 dynamics (Azzaro, 1999; Azzaro et al., 2000).

60 The TFS shows right-lateral and normal dip-slip kinematics and each fault segment is characterized

61 by earthquake related displacements of tens of centimeters and aseismic sliding behavior with slip

62 rates of few mm/year (Bonforte et al., 2011; Azzaro, 2004).

63 Shallow seismicity (< 3 km), associated with these faults, includes the occurrence of several

64 earthquakes with magnitude up to 4.5 (Azzaro et al., 2000) with epicenter in the fault areas. Despite

65 their low-energy release, these events produced destructive effects, with fatalities and injuries, in a

66 very narrow area where they can reach epicentral macroseismic intensity I_0 up to VIII/IX EMS

67 (European Macroseismic Scale, Grünthal, 1998), often accompanied by coseismic surface

68 fracturing (e.g. Azzaro, 1999; 2004) with a mean recurrence time of about 20 years (Azzaro et al.,

69 2013c). The last destructive episodes with I_0=VIII were recorded on 25 October 1984 and 29

70 October 2002. The first is the subject of this work while the second, linked to the SVF dynamics,

71 caused damage at Santa Venerina village (Azzaro et al., 2006; La Delfa et al., 2007).

72 During the second half of October 1984, an anomalous large number of seismic events,

73 concentrated mostly on the eastern side of the volcano, were recorded on Mt. Etna (Gresta et al.,

74 1987). The main events occurred in particular on 19 and on 25 October 1984, respectively at 17.43

75 and 01:11, with epicentral macroseismic intensity I_0 VII (19.10) and VIII (25.10) EMS, which

76 struck the territory of Zafferana and in particular the villages of Fleri and Pisano.

77 The 25 October earthquake was linked to the activity of the Fiandaca Fault (FF) (Azzaro, 1999),

78 while that on 19 October was located in proximity of the Santa Tecla fault (STF). In this paper, we

79   examine the slope distance measurements collected between 1977 and 1985 by a geodimeter

80   trilateration network (Ionica Network, Fig, 2A) set up in 1977 along the eastern edge of the volcano

81   at low altitude (0-700 m b.s.l.) and measured until 1985, to shed new light on the kinematic aspects

82   of this sequence of earthquakes. Indeed, the previously unpublished data, except for an internal

83   report (AA.VV., 1985 in Italian), have been reviewed in the wake of new knowledge acquired in the

84   last two decades, enabling insights into Etna's eastern flank dynamics that were not possible at the

85   acquisition time.

86

87   **2.0 Mt. Etna and its structural framework**

88   Mount Etna (Fig. 1) is a large basaltic volcano built up in a geodynamic setting generated during the

89   Neogene convergence between the African and European plates (e.g. Allard et al., 2006; Branca et

90   al., 2011). It is situated on the eastern coast of Sicily and is one of the most active volcanoes in the

91   world. Mount Etna's activity may be grouped into two types: persistent activity comprising

92   degassing phases alternating with strombolian activity, which may evolve into lava fountains and

93   effusive events, and lateral flank eruptions occurring along fracture systems that are generally

94   preceded by an intrusive process (e.g. Aloisi et al., 2006). The volcano is located at the intersection

95   of two main regional fault systems, having NNW–SSE and NE–SW trends respectively (Fig. 1).

96   The NNW–SSE structural system represents the Sicilian onshore continuation of the Malta

97   Escarpment (ME), the major crustal-scale fault separating the continental African platform from the

98   oceanic Ionian Basin. Ripe Della Naca in Fig. 1 represents surface evidence related to NE-SW

99   Messina-Fiumefreddo (MF) line, while the faults of the "Timpe" system are the major tectonic

100 surface manifestations of the ME. The interaction between regional stress, dike-induced rifting and

101 gravity force is the cause of a fairly continuous and roughly eastward and downward motion of its

102 eastern flank (e.g. Puglisi and Bonforte, 2003; Solaro et al., 2010). This sliding area (Fig. 1) is

103 delimited to the north by the Pernicana–Provenzana Fault System (PFS) (e.g. Obrizzo, 2001;

Natural Hazards
and Earth System
Sciences

Open Access

Discussions

EGU

104   Alparone et al., 2013a), a transtensive E–W trending complex active tectonic structure, while the

105   Trecastagni and Tremestieri faults (e.g. Bonforte et al., 2013) represent the main southern

106   boundaries. The Mt. Etna GPS network has enabled us to determine how the entire eastern flank is

107   affected by an ESE-ward motion, at a mean rate of about 1-3 cm/year (e.g. Bonforte et al., 2011;

108   Gambino et al., 2011). Moreover, starting from 1980, the sliding area underwent two marked

109   acceleration phases in October 1984–1986 and in October 2002 -2005, as described in Alparone et

110   al. (2013c). The authors also highlight a significant temporal correlation between periods of flank

111   acceleration and intensified seismic activity. The TFS is very active from the seismic point of view,

112   both for the number of events and for maximum intensity reached at the epicentre (Azzaro et al.,

113   2013a). TFS is characterized by surface faults of considerable length (up to 8–10 km) and scarps

114   (Azzaro, 1999; Lanzafame et al., 1994). It includes (Fig. 2B) N140°E striking faults (FF, STF and

115   SVF), which define normal right-lateral structures extending from the town of Acireale to Zafferana

116   Etnea and the MF and SLF faults with N160°E structural trend that dissect the base of the volcano's

117   flank by prevailingly vertical movements (Azzaro et al., 2013a).

118   The TFS plays a key role in the local tectonics accommodating the ESE motion; this fault system

119   divides the sliding sector into several blocks (Solaro et al., 2010; Bonforte et al., 2011)

120   characterized by homogeneous kinematics with relative motion measured by Permanent Scatterers

121   (PS) along the faults of about 3-5 mm/years in a "quiet" period such as 1995-2000 (Bonforte et al.,

122   2011).

123

124   **3.0 Mt. Etna seismicity during 1984**

125   In October 1984, an intense seismic sequence was recorded on Mt. Etna area that marked an

126   unusual behavior of the volcano. This swarm comprised more than 1000 earthquakes with M > 2.0

127   over two weeks (16-30 October) and that involved the summit area and almost the entire eastern

128   flank (Gresta et al., 1987; Gresta and Musumeci, 1997).

Natural Hazards
and Earth System
Sciences

Open Access

Discussions

EGU

129   In particular, thousands of events, largely concentrated on the eastern side of the volcano, occurred

130   from October 19 to October 31 (Gresta et al., 1987). The main events (Fig. 2B) were on 19th (at

131   17:43) and 25th October 1984 (at 01:12), and struck the town of Zafferana and the Fleri and Pisano

132   villages (Fig. 3).

133   The earthquakes caused one fatality in Zafferana and injured twelve people in Fleri. In Fleri, the

134   number of injuries would have been much higher, had most of the inhabitants, in great anxiety after

135   an initial shock at around 22.00 the day before, not spent the night outdoors. Serious damage was

136   caused to buildings in Zafferana but particularly in Fleri, which was almost entirely destroyed.

137   About 70% of the buildings of the entire municipality (including all public buildings) were declared

138   unfit for use (Fig. 3).

139   Figure 2 reports the location and epicentral macroseismic intensity (I_0) as reported in the

140   Macroseismic Catalogue of Mt. Etna (CMTE Working Group, 2008). An I_0 of VII EMS (European

141   Macroseismic Scale, Grünthal, 1998) is reported for the October 19th event and of VIII EMS for the

142   October 25th event.

143   In October 1984 more than 1.5 km long NW-SE trending cracks extended from the village of Fleri

144   with dip-slip displacements of about 20 cm. It is worth noting that a similar ground rupture affected

145   the southeastern part of FF on occasion of the VIII EMS event of June 19 1984 (Azzaro, 1999).

146   The volcanic district of Mt. Etna, and in particular its eastern flank, is affected by earthquakes

147   characterized by a strong attenuation of seismic energy in an orthogonal direction to the fault plane.

148   This produces damage extending along narrow zones (1-5 km long, up to 1 km wide) around the

149   seismogenic source (Azzaro et al., 2006) and coseismic surface faulting effects, reported in detail in

150   historical accounts, for the major seismic events. Regarding FF, earthquakes occurring in 1875,

151   1894, 1907, 1914 and 1931 (Azzaro, 2004) caused NNW-SSE trending fractures that opened for

152   several kilometers with prevailing extensional movement and right-lateral displacements of several

153   centimeters.

Natural Hazards
and Earth System
Sciences
Discussions

154 Figure 2B reports macroseismic and instrumental locations of the main seismic events between May

155 1980 and October 1984 in the TFS area. Given that the macroseismic epicentre is calculated as the

156 barycentre of the data points with intensity I = I_0, I_0-1, the macroseismic location and the

157 instrumental location may be rather different, (Azzaro et al., 2000). Indeed Gresta et al. (1987),

158 using a seismic network of just a few active stations in 1984, estimated a duration magnitude of 4.2

159 and 3.9 for the Zafferana and Fleri earthquakes respectively with different epicentres (Fig. 2B).

160

161 **4.0 The "Ionica" EDM network**

162 Between 1977 and 2002, the monitoring of the horizontal component of ground deformation at Mt.

163 Etna was carried out by trilateration geodetic techniques using EDM (electro-optical distance

164 measurements). Three separate networks were installed on the northeastern, western, and southern

165 flanks (Fig. 1).

166 A fourth EDM network (Ionica Network), was installed and measured for the first time in October

167 1977 (Fig. 1), with the aim of verifying the possible relationships between the regional tectonic

168 activity, highly evident in this area with the presence of numerous structures, and the volcanic

169 activity (Fig. 2B).

170 The Ionica Network was set up along the eastern edge of the volcano, along a line from Catania to

171 Taormina, at low altitude (between 700 and sea level); it consisted of 19 benchmarks and 43 lines,

172 which were measured yearly from 1977 to May 1980.

173 The slope distances were recorded by using an AGA 6BL Laser Geodimeter (Fig. 1), and were

174 corrected for atmospheric conditions considering temperature and atmospheric pressure values

175 acquired at the measurement points. The instrumental error of such measurements is 5 mm plus 1

176 ppm of the surveyed distance.

177 After the Zafferana and Fleri 1984 earthquakes, four measurement surveys were performed in the

178 period October 1984 - March 1985 in the portion of the network (Fig. 2B) covering the area

179 affected by the events. The first survey was made between 26 and 31 October. These measurements

Natural Hazards
and Earth System
Sciences

Discussions

180 involved only the southern part of the network, consisting of 9 benchmarks and 19 lines (Fig. 2B)

181 whose mean length is 4.7 km.

182

183 **4.1 EDM Data**

184 The results obtained from data collected from 1977 until 1985, indicate that the variations of

185 distance with values greater than instrumental error occurred mainly in the period May 1980-

186 October 1984, while distance variations obtained from the comparison with the other surveys are

187 mainly within the error. In particular, changes are up to 108 mm and ten measurements showed

188 variations over 50 mm (Fig. 4). In the previous period (1977-1980), the changes observed are

189 generally within the instrumental error though a trend is detectable for several lines.

190 Ground deformation strain field is given by the uniform strain tensor components ε_{ij} which can be

191 calculated by using variations of slope distances (Jaeger, 1969):

192 $\Delta L_{MN}/L_{MN} = \varepsilon_{11} \cos^2\delta_{MN} + \varepsilon_{22} \sin^2\delta_{MN} + \varepsilon_{12} \sin^2\delta_{MN}$

193 where ΔL_{MN} is the change in length of the line MN (with length L_{MN}) between two points M and N

194 and δ_{MN} is the angle between MN direction and x-axis.

195 This tensor indicates the average deformation occurring between two different surveys in the area

196 covered by the network and provides useful information on the ground deformation regime of the

197 area (e.g. Bonaccorso, 2002). We calculated the principal strain axes (Fig. 2C) drawn from the

198 comparison of the overall measurement interval 1980-October 1984. We obtained a positive

199 extension ($\varepsilon_1 = 17 \pm 4.4$ µstrain) oriented approximately orthogonal to and a contraction ($\varepsilon_2 = -12.2$

200 ± 4.4 µstrain) parallel to the FF and STF fault systems (Fig. 2).

201

202 **5.0 Geodetic Data Modelling**

Natural Hazards
and Earth System
Sciences

Discussions

EGU

203   The surface ground deformation field for the 1980-1984 interval was used as input to

204   constrain isotropic half-space elastic inversion models using Okada's (1992) model. The aim of this

205   inversion is to characterize the FF and STF dynamics during this particular period. Unlike in 1985,

206   several of the geometric parameters of the two considered faults are known today (Azzaro et al.,

207   2013). Hence, reducing the unknowns, enables one to make an inversion of the limited EDM

208   dataset.

209   We fixed the more reliable parameters (Tab. 1), while for the more dubious ones (less

210   precise), we chose to leave them to be free (in a range) during the inversion together with the

211   kinematic parameters.

212   To model the displacements due to each single fault, we adopted the analytical model

213   described in Okada (1992), and to take the simultaneously effects of two (or more) faults into

214   account we used the superposition principle. The Okada equations give the 3D displacement (δ_P) at

215   a point P due to the fault geometry and its kinematic. For a baseline between the points Pi and Pj,

216   we modelled the EDM distance variation as:

217

218     $\Delta_{ij} = \left\| \left(P_i + \delta_{P_i} \right) - \left(P_j + \delta_{P_j} \right) \right\| - \left\| P_i - P_j \right\|,$

219   where $\|\cdot\|$ is the 3-dimensional Euclidean norm operator.

220

221   In particular, we inverted for the parameters reported in gray in Table 1, where the

222   associated ranges are also shown. These values are estimations, calculated from geophysical,

223   geological and historical data; however, not all parameters are available. We excluded all the lines

224   crossing the MF. Thus we had a total of 10 free parameters and 13 EDM measurements. It is worth

225   noting in Table 1 that 5 free parameters reach an extreme in their feasible ranges. Hence, they could

226   be treated as fixed parameters and set to their maximum/minimum possible values. We considered a

227   shear modulus of 10 GPa and a Poisson's ratio of 0.25 (e.g. Bozzano et al., 2013).

Natural Hazards
and Earth System
Sciences

Discussions

Open Access

EGU

228   In order to estimate simultaneously the free geometric parameters and kinematics of both the

229   considered faults, we inverted the EDM data by minimizing the weighted misfit between the

230   measured and calculated distances. Because of the free geometric parameters, the mathematical

231   problem is nonlinear and the adopted minimization algorithm was a hybrid approach of genetic

232   algorithm and pattern search (Audet & Dennis, 2002). The measurements were weighted with their

233   associated instrumental errors expressed in meters by the formula:

234    $\sigma_{\Delta_{ij}} = \sqrt{2}\big(0.005 + 10^{-6}\lVert P_i - P_j \rVert\big).$

235   The square root of 2 is due to the error propagation in calculating the distance variation Δ_{ij}

236   neglecting the displacement.

237   The found model fits the EDM data with a WRMS of 0.98.

238   A Jackknife re-sampling method (Efron, 1982) was used to estimate the error of model

239   parameters. The technique requires several optimization executions, each one deprived of just one

240   measurement in input. The errors at 99% are estimated as 3-times the standard deviation in the set

241   of the found solutions.

242   The final results (Tab. 1 and Fig. 5) are in agreement with the dominant faulting style

243   producing a normal strike-slip movement with 27.6 cm of dextral strike movement and 22.7 cm of

244   normal dip on FF, while we obtained only 6.0 cm of dextral strike slip on STF. A comparison

245   between observed and modeled slope distance is reported in Fig. 6.

246

5.1. Sensitivity analysis

248   We carried out a sensitivity analysis in order to ascertain whether our data could constrain a

249   valid set of fault parameters. We adopted the Sobol' analysis (Sobol', 1990), a variance-based

250   global method to measure sensitivity across the whole input space, deal with nonlinear responses,

251   and estimate the effect of interactions in non-additive systems. The method breaks the variance of

252   the output of the model down into fractions (normalized to 1) which can be attributed (in

253 percentage) to input terms. The Sobol' first-order indices indicate the contribution of the main

254 effect of each input parameter to the output variance, therefore measuring the effect of varying the

255 input parameter alone, averaged over variations in other input parameters. We adopted the

256 algorithm in Cannavò (2012) to calculate the first-order Sobol' indices of all the fault parameters

257 given in our EDM data. The indices reported in Table 2 represent the fraction of variance in the data

258 that can be attributed to each fault parameter. The higher the fraction, the more constrained is the

259 parameter by the data. Results show that, among all the parameters, the data are more sensitive to

260 fault lengths and mainly to strike-slips which, in turn, can be estimated more accurately than the

261 other parameters.

262

263 **6.0 Discussion and conclusions**

264   The Timpe is a normal fault system dissecting the Mt. Etna's lower eastern flank. It is

265 formed of several segments (FF, STF, SVF, SLF and MF) that show right-lateral kinematics and

266 normal dip-slip with slip-rates ranging from 3.0 to 5.0 mm/y (Bonforte et al., 2011).

267   Timpe dynamics are linked to the ESE-ward motion of the eastern flank of Mt. Etna (e.g.

268 Azzaro, 2013a). Since 1980, the ESE-ward motion has shown phases of increased velocity, the first

269 being observed in the October 1984-1987 period (Alparone et al., 2013c). The TFS accommodates

270 this motion and becomes very active from the seismic point of view when acceleration phases

271 characterize the ESE-ward motion of the eastern flank.

272   These severe/destructive events, with a mean recurrence time of about 20 years for Azzaro

273 et al. (2013c), make the Timpe fault system extremely important in terms of seismic hazard.

274   These events are distributed on the several segments and in the last decades the destructive

275 episodes have affected FF in October 1984 and SVF in November 2002.

276   The 25th October 1984 event most likely represents the strongest event recorded on FF since

277 1875 (Azzaro et al., 2004); we tried to characterize the finite fault geometry and slip of FF by

Natural Hazards
and Earth System
Sciences
Discussions
EGU

278 ground deformation observations. We recovered and analyzed the EDM measurements of the

279 "Ionica" network crossing the TFS and measured only between 1977 and 1985. These data

280 highlight major variations between 1980 and 1984; the principal components of the strain tensor

281 obtained in this time period, show a positive extension oriented approximately orthogonal and a

282 negative extension parallel to the FF and STF fault systems and are consistent with normal right-

283 lateral dynamics of the two structures.

284   We inverted data showing that, between 1980 and November 1984, the FF (7 km length and

285 2.6 km depth) was affected by a strike slip component of 26.7±1.5 cm and a normal dip slip of

286 22.7±2.4 cm (overall displacement ca. 35 cm). The sensitivity analysis indicates that fault length

287 and strike-slip represent the most accurately constrained parameter obtained by data inversion.

288   In consideration of these results, and assuming a medium rigidity (μ) of a shear modulus of

289 10 GPa in the general relation (Aki, 1966):

290

291      $Mo = \mu * S * \bar{u}$

292   we obtained a geodetic moment $M_G = 6.0 * 10^{23}$ dyne-cm.

293   An estimate of the seismic moment release associated with the seismic events was obtained

294 using the relation (Giampiccolo et al., 2007) for Etnean earthquakes:

295

296      $Log(Mo) = (17.60 \pm 0.37) + (1.12 \pm 0.10) * M_L$

297   It shows that Mo cannot be greater than = $1.6 * 10^{23}$ dyne-cm for the 25 October 1984

298 earthquake and $4.0 * 10^{22}$ dyne-cm for that on 19 June 1984.Therefore only a part (from 5% to a

299 maximum of 30%) of the stick-slip obtained by modeling is related to the co-seismic effects of the

300 earthquakes recorded along the FF, suggesting that most of the slip over the fault must be aseismic.

301 These results are similar to those obtained by Obrizzo et al., (2001) for the Pernicana Fault System,

302 on analyzing 17 years of levelling data. These authors concluded that only 30% of the total

303 deformation of Pernicana Fault System is attributable to co-seismic displacements.

Natural Hazards
and Earth System
Sciences
Discussions

304   Data inversion cover a long period (1980-84); however from May 1980 to May 1984, no events

305   with epicentral intensities $I_0 \geq$ VI EMS were recorded (Fig. 2B) along FF that probably was only

306   subjected to a few centimeters of aseismic displacement (taking in consideration the 3-5 mm/year

307   measured by PS by Bonforte et al., (2011). An acceleration of the FF dynamics could have occurred

308   since June 1984 when an EMS VII was recorded on southeastern part of the fault (Fig. 2B) or after

309   October, 16 when more than 1000 earthquakes with M > 2.0 took place on the eastern flank in two

310   weeks. Field observations certainly suggest that co-seismic ground displacements are larger than

311   what would be expected from the June 19 and October 25 earthquakes. If we exclude any coseismic

312   effect, it is difficult to determine when the dynamics of the FF underwent an acceleration in June-

313   October 1984. If this were the case, it could mean that a destructive seismic event, such as the 25

314   October 1984 one, might have been preceded by a measurable increase of the ground deformation

315   close to the fault.

316   Few variations have been detected on the Santa Tecla Fault (STF), which seems to have been little

317   affected by the October 1984 dynamics. The June 19 event does actually appear to be located at the

318   northern edge of the fault (Gresta et al., 1987). The model estimated only 6.0 (±2.0) cm of strike

319   slip on STF. Then the October 19 event does not seem related to significant shifts of the STF.

320   Precise locations of the earthquakes (M_{max}=3.7) recorded in the same area between 1995 and 2006

321   (Alparone and Gambino, 2003; Alparone et al., 2013b) have shown that the seismicity in this sector

322   is generally 3-5 km b.s.l. deep and related to NE-SW oriented seismogenetic structures (MF line).

323   For all these reasons we retain that the October 19 event is not attributable to TDF dynamics.

324   To summarize, the destructive 25 October 1984 event is an effect of an important dynamic episode

325   that affected the FF structure time related with a flank acceleration phase (Alparone et al., 2013c).

326   EDM data inversion indicated a total stick-slip of ca. 30-35 cm between 1980 and 1984, mainly

327   between June and October 1984 along a fault length of 7 km. This result is in some ways

328   comparable with field observations that detected a co-seismic ground rupture of the northwestern

Natural Hazards
and Earth System
Sciences

Open Access

Discussions

EGU

329 and southeastern sectors of the fault of up to 20 cm (Azzaro, 1999 and reference therein), while a

330 discrepancy between the seismic and geodetic moment is present. Indeed, FF shows a low seismic

331 efficiency (lower than 30%), a feature that seems common to other very shallow faults on the

332 eastern flank (e.g. the Pernicana Fault System) and that highlights that most of the energy is

333 involved in aseismic ground displacements.

334 These considerations again confirm the high level of seismic risk, in particular ground rupture

335 hazard of the Fiandaca Fault and generally of the Timpe Fault System, for the several towns and

336 villages located on these structures.

337 **Acknowledgements**

340

341

342 **References**

343 AA. VV. 1985. Rapporto trimestrale sullo stato dell'attività nell'area etnea. Trimestre ottobre-dicembre

344 1984. Gruppo Nazionale per la Vulcanologia: Unità di ricerca dell'Istituto Internazionale di

345 Vulcanologia, CNR e dell'Istituto di Scienze della terra, Università di Catania.

346 Aki, K., 1966. Generation and propagation of G waves from Niigata earthquake of June 16, 1964,

347 II, Estimation of earthquake moment, released energy, and stress-strain drop from the G wave

348 spectrum, Bull. Earthquake Res. Inst. Univ. Tokyo, 44, 73-88.

349 Allard, P., B. Behncke, S. D'Amico, M. Neri and S. Gambino , 2006. Mount Etna 1993-2005: anatomy of an

350 evolving eruptive cycle, Earth-Sci. Rev., 78, 85-114; doi:10.1016/j. earscirev.2006.04.002.

351 Aloisi, M., Bonaccorso, A., Gambino, S., 2006. Imaging compositive dike propagation (Etna, 2002 case). J.

352 Geophys. Res. 111, B06404. http://dx.doi.org/10.1029/2005JB003908.

353 Alparone, S. and S. Gambino, S., 2003. High precision locations of multiplets on south-eastern flank of Mt.

354 Etna (Italy): reconstruction of fault plan geometry, Physics Earth and Planetary Interiors, 135, 281-

355 289.

356 Alparone, S., O. Cocina, S. Gambino, A. Mostaccio, S. Spampinato, T. Tuvè and A. Ursino, 2013a.

357 Seismological features of the Pernicana-Provenzana fault system and implications for the dynamics of

Natural Hazards
and Earth System
Sciences

Open Access

Discussions

EGU

358   northeastern flank of the volcano, Journal of Volcanology and Geothermal Research, 251, 16-26.
359   doi:10.1016/j.jvolgeores.2012.03.010.

360   Alparone, S., D'Amico, S., Gambino, S., Maiolino V. 2013b. Buried active faults in the Zafferana Etnea
361   territory (south-eastern flank of Mt. Etna): geometry and kinematics by earthquake relocation and
362   focal mechanisms. Annals of Geophysics 56 (1), R0112.

363   Alparone, S., A. Bonaccorso, A. Bonforte, and G. Currenti 2013c, Long-term stress–strain analysis of
364   volcano flank instability: The eastern sector of Etna from 1980 to 2012, J. Geophys. Res. Solid Earth,
365   118, 5098–5108, doi:10.1002/jgrb.50364.

366   Audet, C., & Dennis Jr, J. E. 2002. Analysis of generalized pattern searches. SIAM Journal on Optimization,
367   13(3), 889-903.

368   Azzaro, R. 1999. Earthquake Surface Faulting At Mount Etna Volcano (Sicily) And Implications For Active
369   Tectonics, Journal of Geodynamics, 28 (2-3), 193-213.

370   Azzaro, R., M.S. Barbano, B. Antichi and R. Rigano 2000. Macroseismic catalogue of Mt. Etna earthquakes
371   from 1832 to 1998, Acta Vulcanologica, 12 (1-2), 3-36.

372   Azzaro, R. 2004. Seismicity and active tectonics in the Etna region: constraints for a seismotectonic model,
373   in Mt. Etna: volcano laboratory, Bonaccorso A., S. Calvari, M. Coltelli, C. Del Negro and S.
374   Falsaperla (Editors), American Geophysical Union, Geophysical monograph, 143, 205-220.

375   Azzaro, R., S. D'Amico, A. Mostaccio, L. Scarfì and Y. Tuvè 2006. Terremoti con effetti macrosismici in
376   Sicilia Orientale - Calabria Meridionale nel periodo Gennaio 2002 – Dicembre 2005, Quaderni di
377   Geofisica, 41, 1-60.

378   Azzaro, R., D'Amico, S., Peruzza, L., Tuvè, T., 2012. Earthquakes and faults at Mt. Etna:problems and
379   perspectives for a time-dependent probabilistic seismic hazard assessment in a volcanic region.
380   Bollettino di Geofisica Teorica ed Applicata (1), 75–88.

381   Azzaro R., A. Bonforte, S. Branca, F. Guglielmino 2013a. Geometry and kinematics of the fault systems
382   controlling the unstable flank of Etna volcano (Sicily). J. Volc. Geotherm. Res.251, 5–15.

383   Azzaro R., S. D'Amico, R. Rotondi, T. Tuvè and G. Zonno 2013b. Forecasting seismic scenarios on Etna
384   volcano (Italy) through probabilistic intensity attenuation models: a Bayesian approach J. Volc.
385   Geotherm. Res., 251, 149-157.

386   Azzaro, R., D'Amico, S., Peruzza, L., Tuvè, T., 2013c. Probabilistic seismic hazard at Mt. Etna(Italy): the
387   contribution of local fault activity in mid-term assessment. J. Volc. Geotherm. Res. 251, 158-169.

388   Bonaccorso, 2002. Ground deformation of the southern sector of the Aeolian islands volcanic arc from
389   geodetic data. Tectonophysics, 351- 3, 181-192.

390   Bonforte, A, Puglisi G., 2003. Magma uprising and flank dynamics on Mt. Etna volcano, studied by GPS
391   data (1994–1995). J. Geophys. Res. 108, 2153–2162.

392   Bonforte, A., Guglielmino, F., Coltelli, M., Ferretti, A., Puglisi, G., 2011. Structural assessment of Mt. Etna
393   volcano from Permanent Scatterers analysis. Geochemistry, Geophysics, Geosystems 12, Q02002.
394   http://dx.doi.org/10.1029/2010GC003213.

395   Bonforte, A., Carnazzo, A., Gambino, S., Guglielmino, F., Obrizzo, F., Puglisi, G., 2013. The Trecastagni
396   Fault (Mt. Etna, Italy): a multidisciplinary study by continuous, discrete and satellite ground
397   deformation measurements. Journal of Volcanology and Geothermal Research 251, 42–50.

398   Bozzano, F., Gaeta, M., Lenti, L., Martino, S., Paciello, A., Palladino, D. M., & Sottili, G. 2013. Modeling
399   the effects of eruptive and seismic activities on flank instability at Mount Etna, Italy. Journal of
400   Geophysical Research: Solid Earth, 118(10), 5252-5273.

401   Branca et al., Coltelli M., Groppelli G., 2011. Geological evolution of a complex basaltic stratovolcano:
402   Mount Etna, Italy. Ital. J. Geosci., 130, 306-317.

403   Cannavó, F. 2012. Sensitivity analysis for volcanic source modeling quality assessment and model selection.
404   Computers & Geosciences, 44, 52-59.

405   CMTE Working Group, 2008. Catalogo Macrosismico dei Terremoti Etnei, 1832-2008, INGV, Catania,
406   http://www.ct.ingv.it/ufs/macro/

407   Efron, B., 1982. The Jacknife, Bootstrap and Other Resampling Plans. Philadelphia: Society for Industrial
408   and Applied Mathematics.

409   Gambino, S., Bonforte, A., Carnazzo, A., Falzone, G., Ferrari, F., Ferro, A., Guglielmino, F., Laudani, G.,
410   Maiolino, V., Puglisi, G., 2011. Displacement across the Trecastagni Fault (Mt. Etna) and induced
411   seismicity: the October 2009–January 2010 episode. Ann. Geophys., 54, 414–423.

412   Giampiccolo, E., S. D'Amico, D. Patanè, and S. Gresta, 2007, Attenuation and source parameters of shallow
413   microearthquakes at Mt. Etna Volcano, Italy, Bull. Seismol. Soc. Am., 97, 184–197,
414   doi:10.1785/0120050252.

415   Gresta, S., Glot, J.P., Patanè, G., Poupinet, G., Menza, S., 1987. The October seismic crisis at Mount Etna.
416   Part I: Space-Time evolution of events. Ann. Geophys. 5B (6), 671–680.

417   Gresta, S., Musumeci, C., 1997. Stress tensor computation from earthquake fault-plane solutions: an
418   application to seismic swarms at Mt. Etna volcano (Italy). Annali di Geofisica, XL, 5, 1250-1260.

419   Grünthal, G. (ed) 1998. European macroseismic scale 1998 (EMS-98). European Seismological
420   Commission, subcommission on Engineering Seismology, working Group Macroseismic Scales.
421   Conseil de l'Europe, Cahiers du Centre Européen de Géodynamique et de Séismologie, 15,
422   Luxembourg, 99 pp

423   Jaeger, J.C., 1969. Elasticity, Fracture and Flow. With Engineering and Geological Applications. Chapman
424   & Hall, London, 268 pp.

425   La Delfa S, Patanè G, Presti F, Tringali G. 2007. Changing in crust mechanical behaviour due to raising
426   magma: a fracturing model of SE flank of Mt Etna (Sicily). Earth Planet Sci Lett 256:493–509

427   Lanzafame, G., M. Neri and D. Rust, 1994. Active tectonics affecting the eastern flank of Mount Etna:
428   structural interactions at a regional and local scale, in Etna: fifteen years on Gravestock, P.J. and W. J.
429   Mc Guire, (Editors.), Cheltenham and Gloucester Special Publication, 25-33.

430   Obrizzo, F., Pingue, F., Troise, C., De Natale, G., 2001. Coseismic displacements and creeping along
431   Pernicana fault (Mt. Etna) in the last seventeen years: a detailed study of a structure on a volcano.
432   Journal of Volcanology and Geothermal Research 9, 109–131.

433   Okada, Y. 1992. Internal deformation due to shear and tensile faults in a half-space. Bull Seism Soc Am
434   82(2), 1018-1040.

435   Sobol', I. Y. M. 1990. On sensitivity estimation for nonlinear mathematical models. Matematicheskoe
436   Modelirovanie, 2(1), 112-118.

437   Solaro, G., V. Acocella, S. Pepe, J. Ruch, M. Neri, Sansosti E. 2010. Anatomy of an unstable volcano from
438   InSAR: Multiple processes affecting flank instability at Mt. Etna, 1994-2008, Journal of Geophysical
439   Research, 115, B10405, doi:10.1029/2009JB000820.

Natural Hazards
and Earth System
Sciences
Open Access
Discussions

440
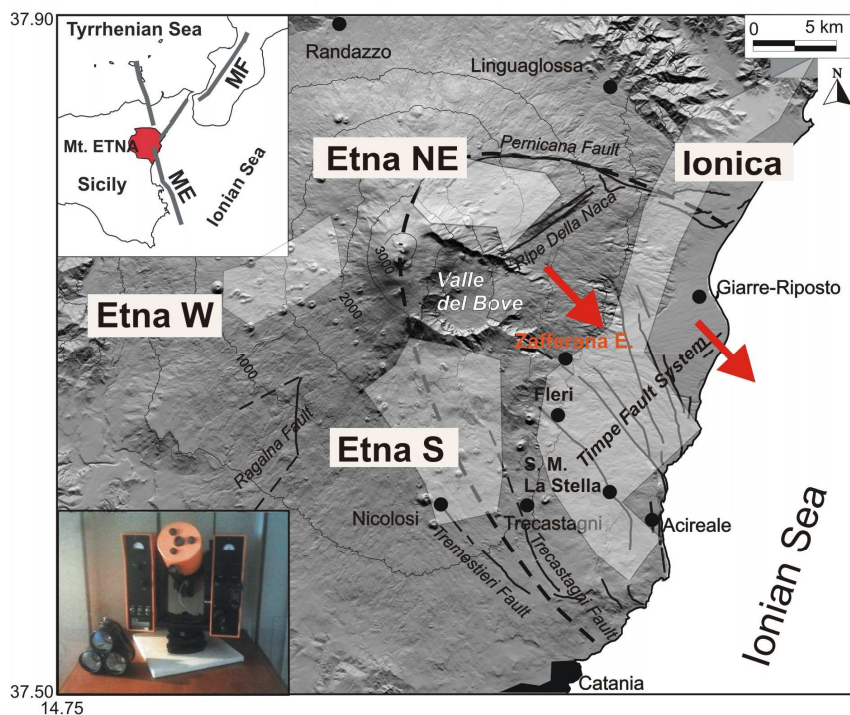
Fig. 1 –Surface faults map of Mt. Etna. Top inset map shows the main regional fault

systems: MF=Messina-Fiumefreddo line, ME=Malta Escarpment. Dashed line defines the

sliding sector and red arrows indicate its movement direction. White areas are covered by EDM

networks. In the bottom insert, the AGA 6BL Laser Geodimeter.

445
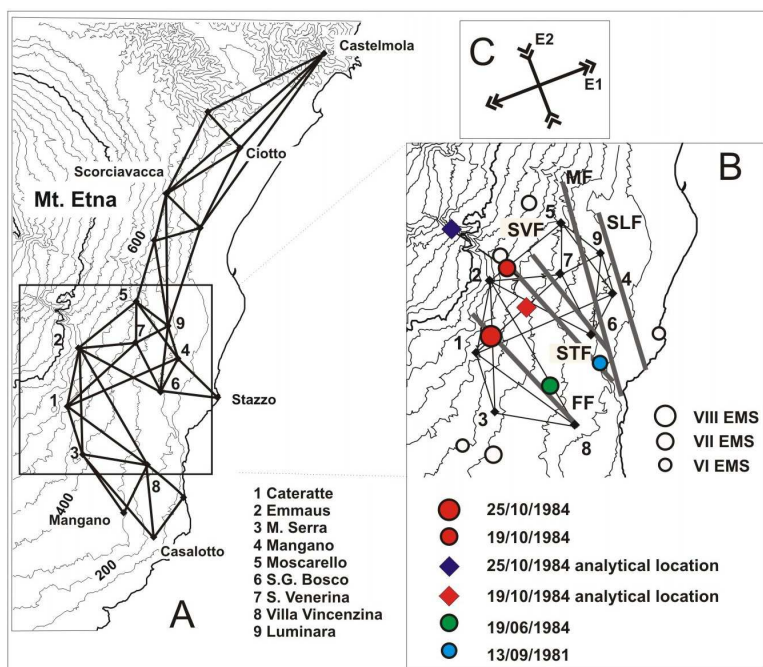
Fig. 2. – Ionica EDM network (a) EDM benchmarks and lines measured between 1977 and
1985 (b) Macroseismic epicentres of earthquakes with epicentral intensities $I_0 \geq$ VI EMS occurring
from 1980 to October 1984 in the south-eastern flank of Mt Etna. (c) Principal strain axes obtained
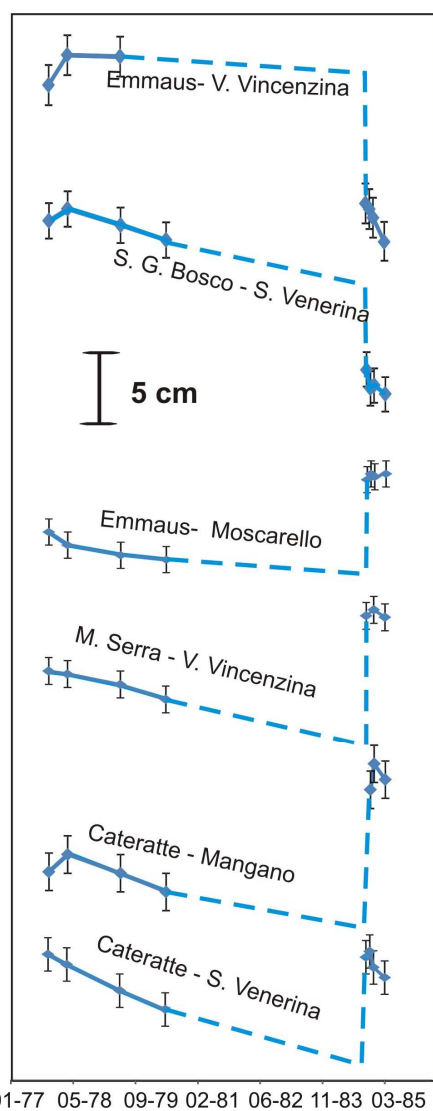from the comparison of the overall measurement interval 1980-October 1984.

450

Fig. 3. Photos of damage caused during the 25th October earthquake at Fleri village
(http://www.ct.ingv.it/macro/etna/html_index.php).

Natural Hazards
and Earth System
Sciences

Discussions

Open Access

EGU
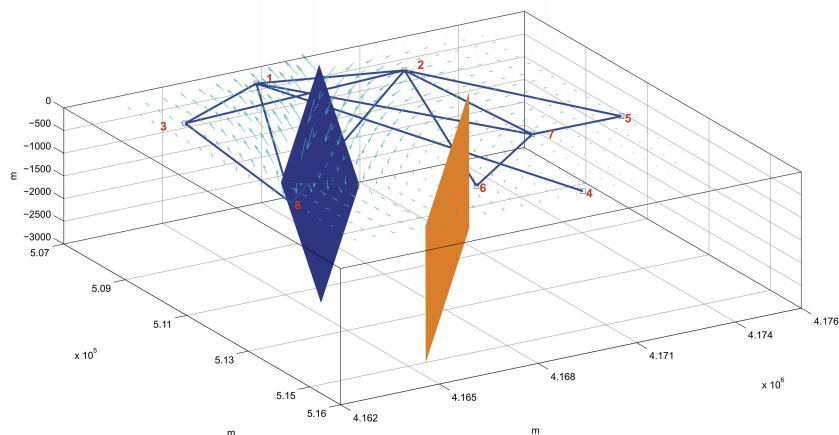
453

Fig. 4. Changes of measured line lengths with respect to time of surveying time (interval 1977– 1985) in the "Ionica" network. Note how the lines are subject to marked variations in the 1980-1984 period. Solid lines connect measurements and dashed lines represent the plausible trend of the May 1980-October 1984 period.
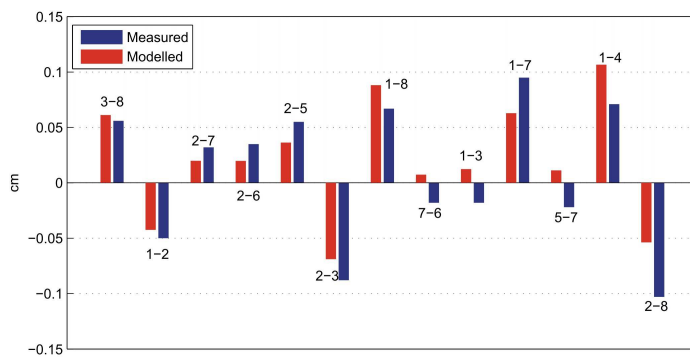
459

460

461

462

Fig. 5. Location and E-W cross-section of the source modelled. The arrows represent the simulated deformation field due to the estimated fault kinematics. Numbers as in Fig. 2.

465

Fig. 6. Comparison between observed (blue bars) and modeled (red bars) slope distance. Numbers as in figure 2.

468

469

470

471

21

Natural Hazards
and Earth System
Sciences

Open Access

EGU

Discussions

472

473   **Table 1.** Best Fitting Range for the model.

	Fault 1 (FF)		Fault 2 (STF)	
X (m, center top)	509700	fixed	512423	fixed
Y (m, center top)	4166660	fixed	4168595	fixed
Depth (m, top)	0	fixed	0	fixed
Azimuth (°)	140	fixed	140	fixed
Dip (°)	70 ± 0.0	70 ÷ 89.9	89.9 ± 25	70 ÷ 89.9
Semi-Length (m)	3500 ± 0.0	2000 ÷ 3500	4000 ± 0.0	2000 ÷ 4000
Width (m)	2610 ± 70	1000 ÷ 3000	3000 ± 100	1000 ÷ 3000
Strike-s (cm)	26.7 ± 1.5	0 ÷ 100 (dextral)	6.0 ± 2.0	0 ÷ 100 (dextral)
Dip Slip (cm)	-22.7 ± 2.4	-100 ÷ 0 (normal)	0.0 ± 3.0	-100 ÷ 0 (normal)

474

475   **Table 2.** Global sensitivity analysis. First-order Sobol' coefficients for the fault parameters
476   and total sums**.**

	Fault 1 (FF)	Fault 2 (STF)	TOTAL
Azimuth (°)	0.000	0.002	0.002
Dip (°)	0.000	0.005	0.005
Semi-Length (m)	0.119	0.126	0.245
Width (m)	0.012	0.019	0.031
Strike-s (m)	0.125	0.284	0.409
Dip Slip (m)	0.013	0.014	0.027
TOTAL	0.269	0.450	

477